DISPERSION OF UNDER-EXPANDED HYDROGEN-METHANE BLENDED JETS THROUGH A CIRCULAR ORIFICE

Gopakumar Ramachandran, Ethan S. Hecht

Combustion Research Facility, Sandia National Laboratories, Livermore, CA, USA- 94551

gramach@sandia.gov, ehecht@sandia.gov

ABSTRACT

Blending hydrogen into natural gas and using existing natural gas infrastructure provides energy storage, greenhouse gas emission reduction from combustion, and other benefits as the world transitions to a hydrogen economy. Though this seems to be a simple and attractive technique, there is a dearth of existing safety codes and standards and understanding the safety implications is warranted before implementation. In this paper, we present some preliminary findings on the dispersion characteristics of hydrogen-methane blends performed under controlled conditions inside a laboratory. Experiments were performed at two different upstream pressures of 5 and 10 bar as the blends dispersed into air through a 1 mm diameter orifice. Blends of 25, 50, and 75 vol-% hydrogen in methane were tested. Spatially resolved Raman signals from hydrogen, methane and nitrogen were acquired simultaneously at 10 Hz using separate ICCD cameras from which the individual concentrations and jet boundaries could be determined. Finally, a comparison between dispersion characteristics of blended fuel jets with pure hydrogen and pure methane jets was made.

1.0 INTRODUCTION

Hydrogen, a clean fuel with zero CO_2 emissions, has great potential as a sustainable fuel in the energy and transportation sector, especially for fuel cell vehicles. A complete transition to a hydrogen economy will require major investments in terms of infrastructure development and will require a significant amount of time to attain fruition. The introduction and establishment of a new technology does not necessarily require radical changes but can be achieved by incremental modifications to the existing system [1]. Blending hydrogen with natural gas can serve as an intermediate step in the process of achieving 100% decarbonization.

In United States, there exists a well-established pipeline network for transporting natural gas and there are proposals to utilize these pipelines for hydrogen. This can significantly reduce the lead time for infrastructure development and lower project expenses. When hydrogen is introduced into natural gas pipelines, the resultant mixture exhibits different properties [2]. Since hydrogen is lighter than methane (the primary molecule in natural gas), the density of the blended mixture is reduced. For a given pressure and leak size, the volumetric flow rate of a blended fuel will be greater than the equivalent leak of pure methane [3], with the potential to generate a combustible cloud whose accidental ignition could be hazardous. It is important to understand the dispersion and ignition characteristics of blends so that the hazards can be appropriately controlled, and safety, codes and standards can be established.

A substantial amount of numerical [4-7] and experimental [8-23] studies have been reported on the dispersion and/or ignition behavior of hydrogen and/or methane jets, including cryogenic releases [18-21], but very limited data is available on the behavior of unignited blends released at high pressure. In the present

study, the concentration statistics of hydrogen and natural gas blended at different proportions are obtained downstream of a 1 mm diameter orifice at 5 bar and 10 bar conditions using planar laser Raman scattering.

2.0 EXPERIMENTAL AND OPTICAL SETUP

The dispersion studies were conducted at the Turbulent Combustion Laboratory of Sandia National Laboratories. The details of the experimental and optical setup are illustrated in Figure 1. The pressure of the gas (hydrogen, blend, or methane) in a settling chamber is controlled as the gas is released into the ambient through a circular orifice of 1 mm diameter. A linear translation stage enables movement of the setup along three orthogonal axes and this enables measurements at different heights (or planes) without altering the position of the diagnostics. An active exhaust hood above the release is used to expel the unburned gases outside the lab. The fuel valves, pressure regulators, flow controllers and the translation stage are controlled using a LabView program.

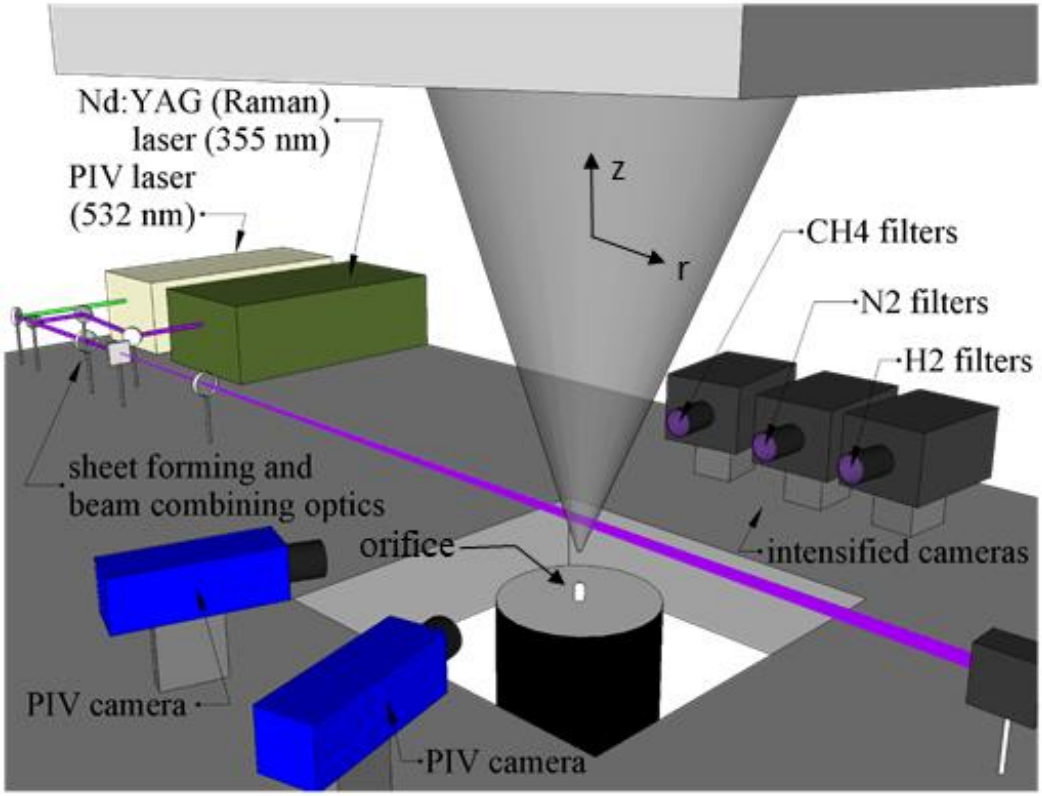

Figure 1. Experimental and optical setup used for release experiments.

The third harmonic of a pulsed Nd:YAG laser (Continuum PL-9010) with a pulse width of 7 ns and approximately 450mJ/pulse is used to excite the gas molecules. The circular beam is converted into a sheet and is directed into the region of interest using a combination of a cylindrical lens (f =-200 mm) and a spherical lens (f =1000 mm). Raman signals from the molecules of interest (namely hydrogen, nitrogen and methane) are captured using Princeton Instruments Intensified CCD cameras, mounted with 50 mm lenses. The camera lenses are outfitted with bandpass filters (420 ± 10 nm for H_2, 387 ±10 nm for N_2 and 400 ± 10 nm for CH_4) to restrict other wavelengths and 355 nm notch filters (OD 6) to minimize observed Rayleigh or background scattered light. Focusing issues due to camera inclination relative to the laser sheet are

corrected using Schiempflug principle. The images are corrected for pulse-to-pulse variations and laser non-uniformities in the vertical direction after removing the background noise using an in-house Python program. Since the Raman scattering cross section is at least 3 orders of magnitude smaller than Rayleigh, the sheet size cannot be too large and is kept at 30 mm to improve the signal-to-noise ratio.

To prevent the cameras from observing the laser scatter from the nozzle, measurements were initiated at a height of 16 mm above the orifice. The setup is traversed downward vertically in increments of 25 mm to obtain the concentration fields up to the height of 210 mm. Data at each height consists of 400 images for each species, acquired simultaneously, to obtain the two-dimensional multi-scalar fields. These scalar field images at eight different heights were stitched together to reconstruct the overall concentration profiles corresponding to a particular species of interest. It should be noted that the simultaneous measurements of hydrogen and methane mole fraction fields are limited only to the blends, while 100% hydrogen and 100% methane cases are measured separately.

3.0 RESULTS AND DISCUSSION

This study focuses on understanding the dispersion characteristics of pure hydrogen, pure methane and hydrogen-methane blends at various proportions (75% H_2 -25% CH_4, 50% H_2 -50% CH_4 and 25% H_2 -75% CH_4**)** at 5 bar and 10 bar pressures through a circular orifice of 1 mm diameter as summarized in Table 1.

Table 1. Test conditions.

Gas Composition	**Pressures**	**Orifice Diameter**
100% H_2	5 bar, 10 bar	1 mm
75% H_2 -25% CH_4	5 bar, 10 bar	1 mm
50% H_2 -50% CH_4	5 bar, 10 bar	1 mm
25% H_2 -75% CH_4	5 bar, 10 bar	1 mm
100% CH_4	5 bar, 10 bar	1 mm

3.1 SPECIES CONCENTRATION DISTRIBUTION

Figure 2 shows the median mole fraction fields corresponding to 10 bar pressure conditions. The orifice is located at (0, 0); the images start axially 16 mm downstream of the orifice as mentioned in Section 2.0. The set of four images on the left shows the mole fraction of hydrogen while the methane mole fraction fields are shown on the right. The stitched images appear to be fairly smooth for hydrogen, while the methane images are noisier. This noise is particularly evident where the different heights are stitched together, especially further downstream along the jet axis. As would be expected, the pure hydrogen or methane jets have the highest mole fraction fields, and as the hydrogen or methane concentration of the mixture decreases, so does the mole fraction intensity. All of the jets have a similar, expected shape with high concentration near the nozzle that spreads out downstream as air is entrained and mixing progresses. Future work will attempt to improve the quality of this data using filtering as described by Li et al. [18].

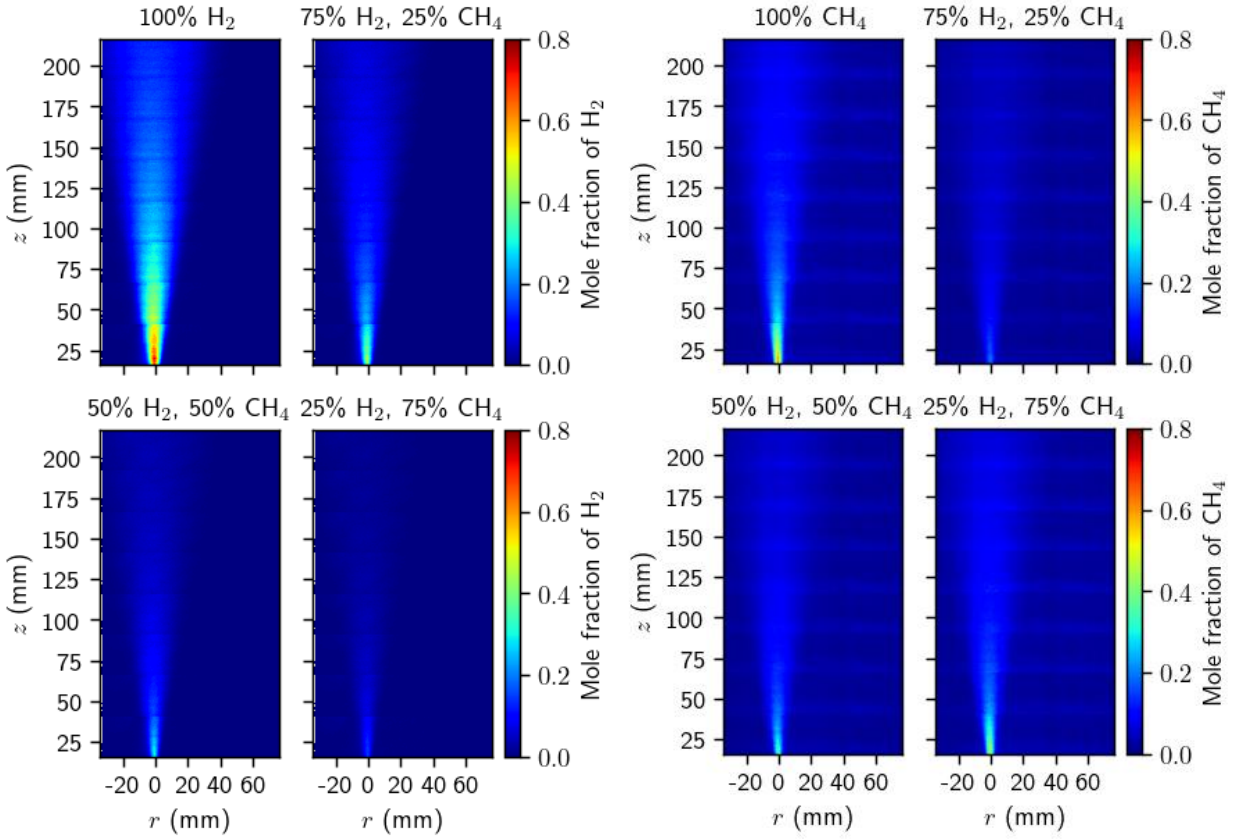

Figure 2. Hydrogen (left) and methane (right) mole-fraction fields at 10 bar pressure for the gas compositions listed in Table 1.

3.1.1 Axial distribution

The variations in median centerline mole fractions of hydrogen and methane are shown in Figure 3. For the conditions mentioned in Table 1, there exists a monotonic decrease in concentration of both the species along the jet centerline. The concentration profiles decay hyperbolically for all the blends; consistent with the behavior of pure hydrogen and methane reported in the present work and other literature [10, 13, 18-21]. The concentration gradient is maximum in the near field of the orifice, especially in the potential core region. Immediately after this zone, which extends several diameters downstream of the jet, the species mole fractions decrease rapidly due to the entrainment of ambient air into the high velocity fuel jet and asymptotically approach zero in the far field region.

For the 100% releases, the methane mole fraction along the centerline decays faster than the hydrogen mole fraction. This is similar to observations by Schefer et al. [13] who observed the mole fraction of lighter gases (i.e., hydrogen) decays slower than higher density gases (i.e., methane). The mass fraction decay rate, on the other hand, will decay faster for hydrogen than methane, owing to the difference in molecular weights and the conversion from mole to mass fraction [13]. The literature has shown the inverse mass fraction decay rate to be constant for a range of gases when appropriately normalized by the effective jet diameter or radius which accounts for the initial density difference of the released gas [10, 13]. For the blends at an equivalent initial mixture mole fraction and pressure, the mole fraction at a downstream point

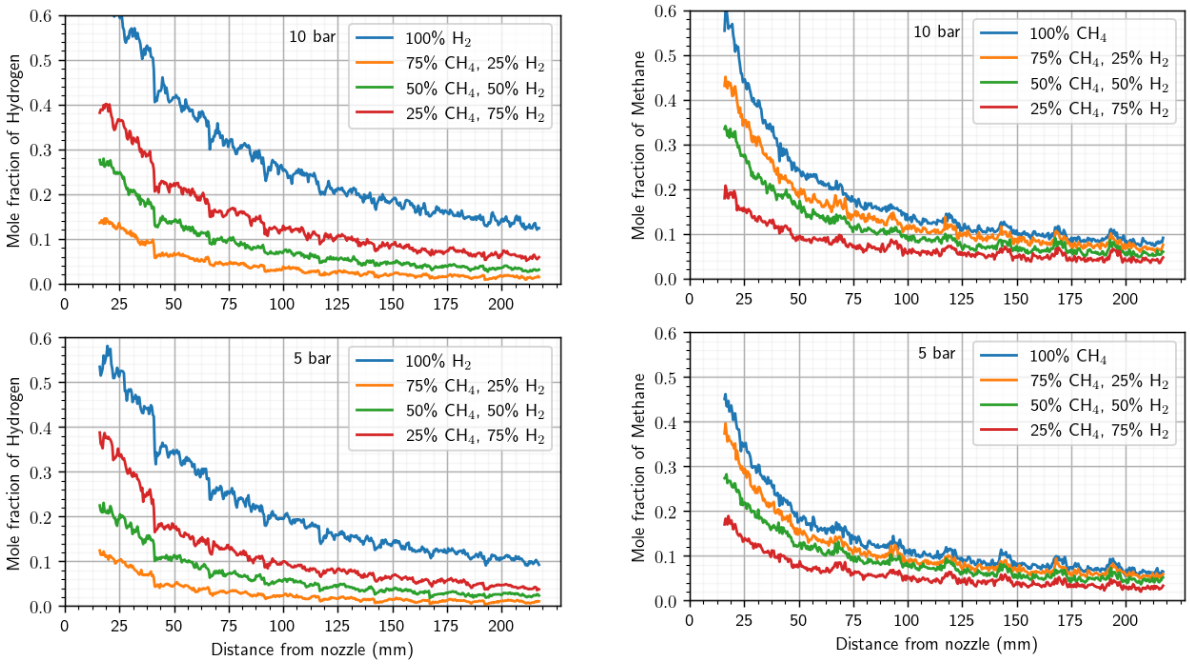

Figure 3. Centerline mole-fractions of hydrogen (left) and methane (right) for different blends at 10 bar (top) and 5 bar (bottom) pressures.

is higher for methane than for hydrogen. It is less obvious in this plot whether the mole fraction decay rate for methane or hydrogen is faster or if they are the same. A comparison of the axial mole fraction ratios is included later in Section 3.2.

3.1.2 Radial Distribution

The radial mole fraction distribution at various horizontal planes downstream of the orifice is shown in Figure 4 and Figure 5. Here the radial distance (r) is normalized by the corresponding axial distance (z) and we plotted this against the mole fraction values normalized using the centerline mole fraction (X_{cl}). At each axial location along the centerline, the mole fraction peaks and decreases radially outwards towards the jet boundary. The results show that the mean radial profile for several downstream distances collapses onto a Gaussian profile for both 5 bar and 10 bar pressure conditions, as has been observed by others (but are typically plotted as mass fraction profiles) [10, 13, 19, 20]. Beyond 150 mm, the data tend to scatter due to reduced signal-to-noise ratio and this effect is predominantly seen with the methane mole fractions due to a lower signal to noise ratio for the methane camera. This confirms the self-similar nature of the blended gas jets, as have been observed for pure hydrogen and methane previously. There does not appear to be a trend with respect to the halfwidth of the profiles (i.e., all of the halfwidths appear to be similar). In future work, the mole fractions will be converted to mass fractions and the self-similar profiles will be compared to the typical Gaussian profile which has a halfwidth of approximately $r/z \cong 0.11$ [10, 18, 19, 20]; the mole fraction halfwidth is obviously significantly wider than this.

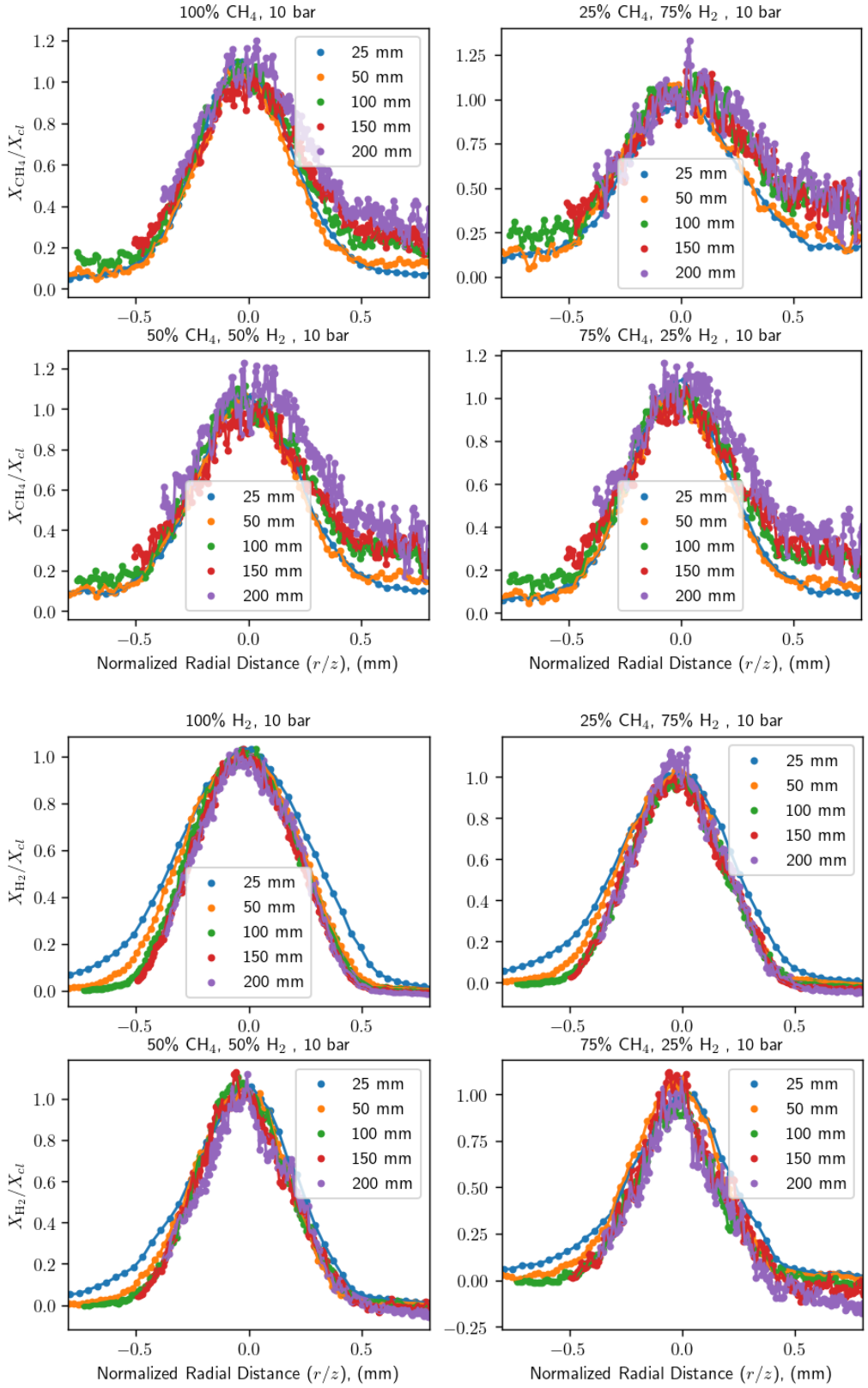

Figure 4. Radial profiles of mole-fraction for 10 bar pressure condition.

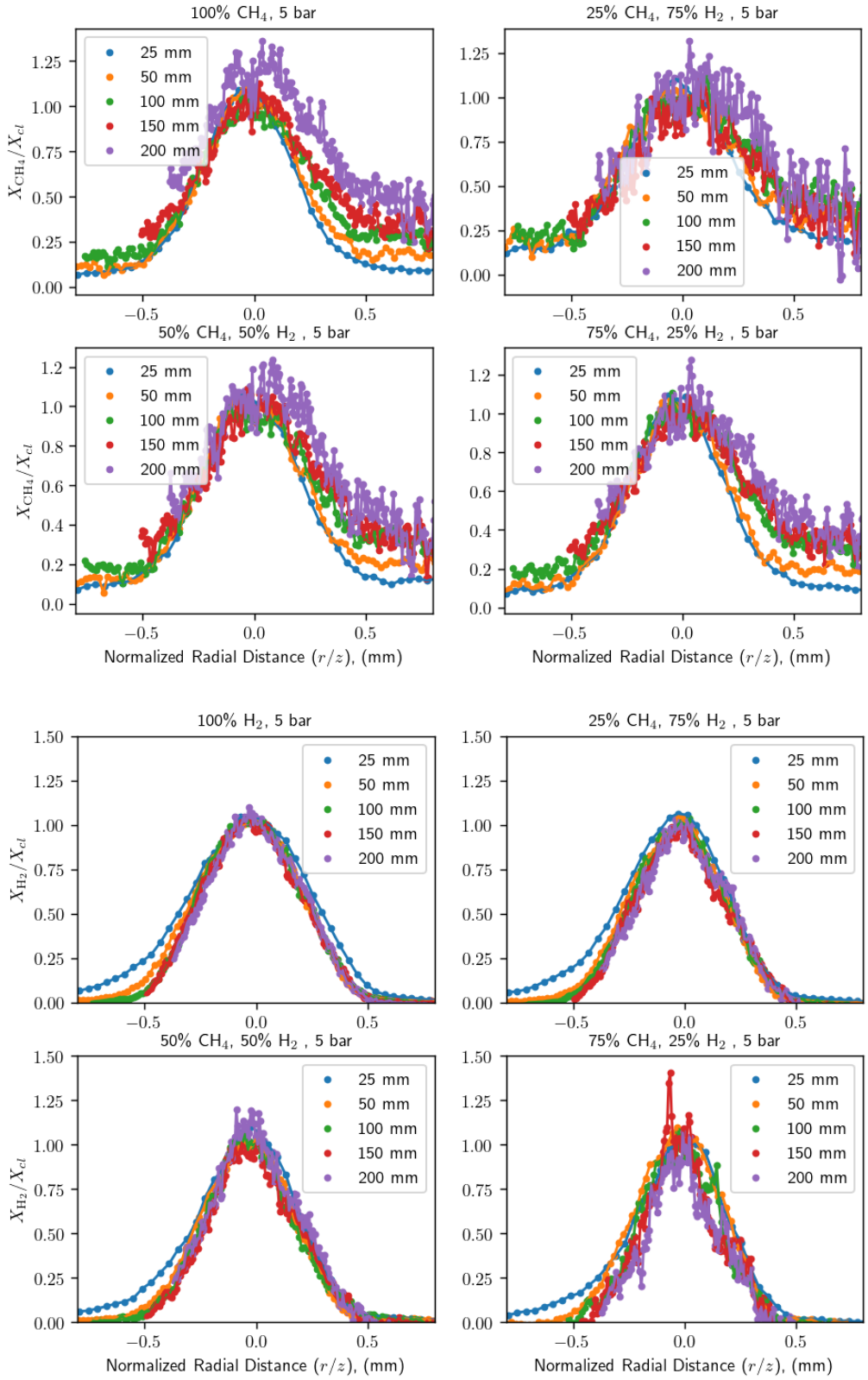

Figure 5. Radial profiles of mole-fraction for 5 bar pressure condition.

3.2 RELATIVE SPECIES CONCENTRATIONS

Figure 6 shows the computed relative mole fractions of methane and hydrogen along the centerline. The plots also show a linear fit of this ratio. The intercept values are near the expected mole fraction ratios at the orifice exit based on the gas concentration (3, 1, and 0.3 for the 75%, 50% and 25% CH_4 blends, respectively), however a perfect match is not observed. This is likely due to noisy data, but could also be because our measurements start at 16 mm downstream of the orifice and the hydrogen diffuses more rapidly

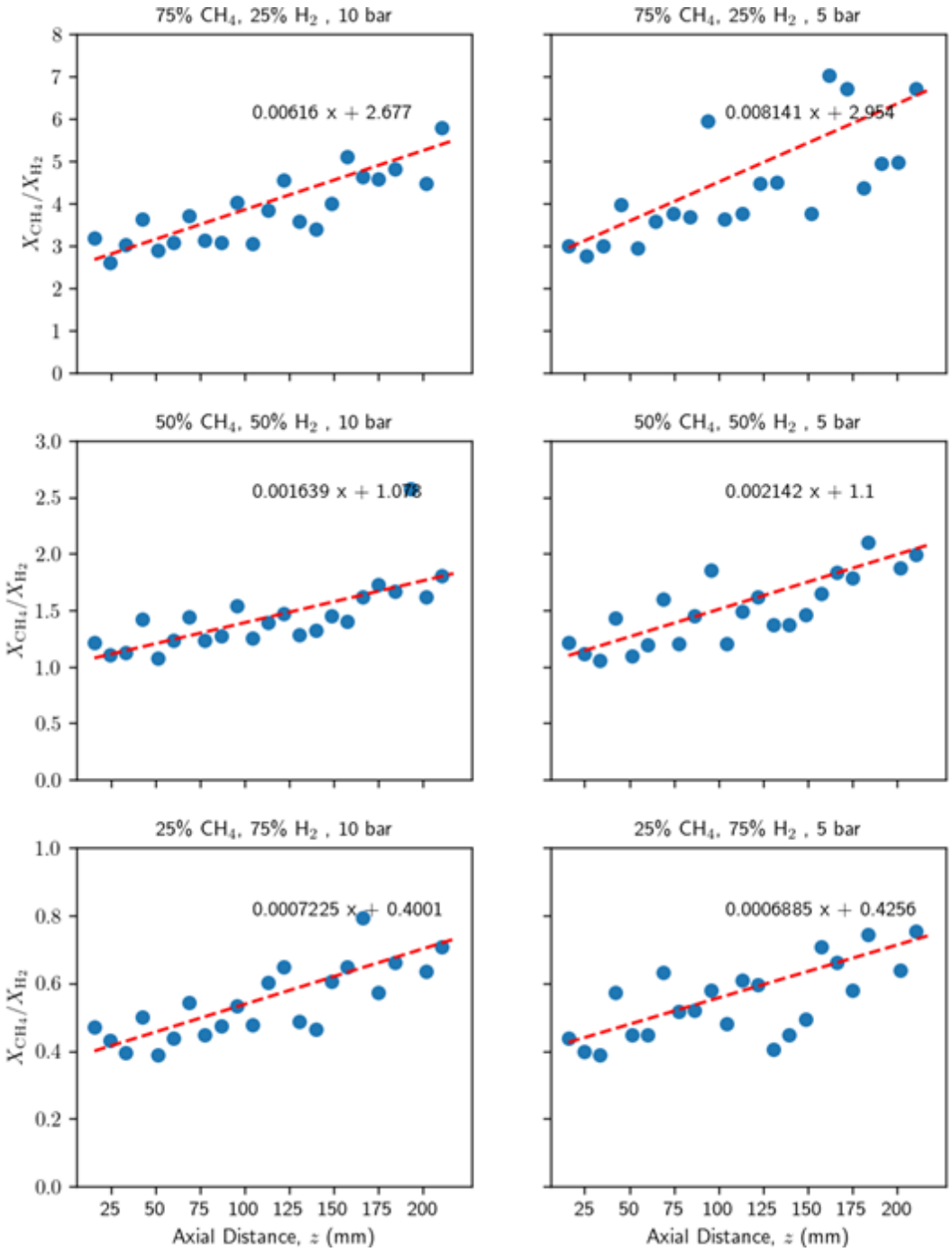

Figure 6. Ratio of CH_4 to H_2 Mole fractions along jet centerline.

than methane, especially in the potential core region, resulting in a slightly higher ratio of methane to hydrogen concentration than what is expected at the orifice exit.

In all cases, the ratio of methane to hydrogen mole fraction along the centerline increases with downstream distance. For both pressures, the rate at which this ratio increases diminish as the mole fraction of hydrogen increases in the initial mixture. The rate of increase is also higher for the 5 bar releases than the 10 bar releases (with the exception of the 25% methane case). This increasing mole fraction ratio may be due to the higher diffusivity of hydrogen over methane. Because the hydrogen moves more rapidly in the radial direction than the methane, there is less hydrogen at further downstream distances than methane. This is supported by the observation that the higher momentum, 10 bar release has less of an influence from diffusion than the 5 bar release and therefore a lower rate of ratio change. As was discussed in Section 3.1.1, conversion to mass fraction will change the decay rate, and the ratio of mass fractions along the centerline will be different than the ratio of mole fractions. Ideally, the mass fraction ratio will remain constant throughout the dispersion profiles and the dispersion can be described by a single mass fraction of fuel to air.

4.0 SUMMARY AND CONCLUSIONS

The dispersion characteristics of different hydrogen-methane blends (75% H_2-25% CH_4, 50% H_2-50% CH_4 and 25% H_2-75% CH_4**)** at 5 bar and 10 bar pressures, released through a 1 mm diameter orifice was studied using planar laser Raman scattering. Two-dimensional concentration fields corresponding to hydrogen and methane were measured simultaneously. The average centerline concentration profiles decayed hyperbolically for all the blends, consistent with the behavior of pure hydrogen and methane. The average centerline methane mole fraction decayed more rapidly than the centerline hydrogen mole fractions for the pure gases. The radial mole fractions, when normalized with centerline mole fraction and radially by downstream distance, collapsed onto a self-similar Gaussian profile for both the pure gases and blends. The ratio of methane to hydrogen mole fractions along the centerline shows a linearly increasing trend, possibly due to increased diffusion rate of hydrogen over methane.

Most of the literature data is reported in terms of mass fraction, and we plan to convert the data from our experiments to mass fraction to see if the same trends for pure gases remain for blends of hydrogen and methane. Of particular interest is whether the same self-similar characteristics for pure gases hold true for blends of hydrogen or methane. This self-similarity depends on the mass fraction ratio of hydrogen to methane remaining constant as air is entrained so that a single blend mass fraction relative to air at any point in the flow can be specified rather than an independent mass fraction of the constituents. This work shows that the mole fraction ratio of hydrogen to methane does not remain constant throughout the flow.

Blend dispersion characteristics have implications for safety and ignitability. This data will be used to validate models for blend dispersion that can also be used in safety assessments of blended gas infrastructure. Relation of the concentration fields to the ignitability of these blends will also be made to provide a basis for codes and standards related to natural gas and hydrogen blends, a stepping-stone to a decarbonized future.

5.0 ACKNOWLEDGEMENTS

This work was supported by the Department of Energy Office of Energy Efficiency and Renewable Energy Hydrogen and Fuel Cell Technologies Office, as part of the Safety Codes and Standards program under the direction of Laura Hill. Sandia National Laboratories is a multi-mission laboratory managed and operated

by National Technology & Engineering Solutions of Sandia, LLC (NTESS), a wholly owned subsidiary of Honeywell International Inc., for the U.S. Department of Energy's National Nuclear Security Administration (DOE/NNSA) under contract DE-NA0003525. This written work is authored by an employee of NTESS. The employee, not NTESS, owns the right, title and interest in and to the written work and is responsible for its contents. Any subjective views or opinions that might be expressed in the written work do not necessarily represent the views of the U.S. Government. The publisher acknowledges that the U.S. Government retains a non-exclusive, paid-up, irrevocable, world-wide license to publish or reproduce the published form of this written work or allow others to do so, for U.S. Government purposes. The DOE will provide public access to results of federally sponsored research in accordance with the DOE Public Access Plan.

REFERENCES

1. A. Marangon and M.N. Carcassi, Hydrogen–methane mixtures: Dispersion and stratification studies, International Journal of Hydrogen Energy 39 (2014) 6160-6168
2. Devinder Mahajan, Kun Tan ,T. Venkatesh, Pradheep Kileti, and Clive R. Clayton, Hydrogen Blending in Gas Pipeline Networks—A Review, Energies 2022, 15, 3582
3. B.J. Lowesmith , G. Hankinson , C. Spataru , M. Stobbart , Gas build-up in a domestic property following releases of methane/hydrogen mixtures, International Journal of Hydrogen Energy 34 (2009), 5932-5939
4. A.G Venetsanos , T Huld , P Adams , J.G Bartzis, Source, dispersion and combustion modelling of an accidental release of hydrogen in an urban environment, Journal of Hazardous Materials 105 (2003), 1-25
5. A.G. Venetsanos, S.G. Giannissi, Release and dispersion modeling of cryogenic under-expanded hydrogen jets, International Journal of Hydrogen Energy, 42 (2017), 7672-7682
6. P. Middha, O.R. Hansen, J. Grune, Alexei Kotchourko, CFD calculations of gas leak dispersion and subsequent gas explosions: Validation against ignited impinging hydrogen jet experiments, Journal of Hazardous Materials 179 (2010), 84-94
7. P. Bénard, A. Hourri, B. Angers, A. Tchouvelev, Adjacent surface effect on the flammable cloud of hydrogen and methane jets: Numerical investigation and engineering correlations, International Journal of Hydrogen Energy 41 (2016), 18654-18662
8. A.D. Birch, D.R. Brown, M.G. Dodson F. Swaffield, The Structure and Concentration Decay of High Pressure Jets of Natural Gas, Combustion Science and Technology, 36 (1984), 249-261
9. A.D. Birch, D.R. Brown, M.G. Dodson, Ignition probabilities in turbulent mixing flows, Symposium (International) on Combustion 18 (1981), 1775-1780
10. C.D. Richards and W.M. Pitts. Global density effects on the self-preservation behaviour of turbulent free jets. Journal of Fluid Mechanics, 254 (1993), 417-435
11. R.W. Schefer, G.H. Evans, J. Zhang, A.J. Ruggles, R. Greif, Ignitability limits for combustion of unintended hydrogen releases: Experimental and theoretical results, International Journal of Hydrogen Energy, 36 (2011), 2426-2435
12. R.W. Schefer, W.G. Houf, T.C. Williams, B. Bourne, J. Colton, Characterization of high-pressure, underexpanded hydrogen-jet flames, International Journal of Hydrogen Energy, 32 (2007), 2081-2093
13. R.W. Schefer, W.G. Houf, T.C. Williams, Investigation of small-scale unintended releases of hydrogen: momentum-dominated regime, International Journal of Hydrogen Energy, 33 (2008). 6373-6384

14. R.W. Schefer, W.G. Houf, T.C. Williams, Investigation of small-scale unintended releases of hydrogen: buoyancy effects, International Journal of Hydrogen Energy, 33 (2008), 4702-4712
15. M.R. Swain, P.A. Filoso, M.N. Swain, An experimental investigation into the ignition of leaking hydrogen, International Journal of Hydrogen Energy, 32 (2007), 287-295
16. A.J. Ruggles, I.W. Ekoto, Ignitability and mixing of underexpanded hydrogen jets, International Journal of Hydrogen Energy, 37 (2012), 17549-17560
17. K. Okabayashi, K. Tagashira, K. Kawazoe, K. Takeno, M. Asahara, A.K. Hayashi, M. Komori, Non-steady characteristics of dispersion and ignitability for high-pressurized hydrogen jet discharged from a pinhole, International Journal of Hydrogen Energy, 44 (2019), 9071-9079
18. X. Li, C. Yao, S.C. Egbert, Q. He, Z. Zhao, D.M. Christopher, E.S. Hecht, Self-similar characteristics of underexpanded, cryogenic hydrogen and methane jets, International Journal of Hydrogen Energy, 48 (2023), 4104-4117
19. E.S. Hecht, P.P. Panda, Mixing and warming of cryogenic hydrogen releases, International Journal of Hydrogen Energy, 44 (2019), 8960-8970
20. Bikram Roy Chowdhury and Ethan S. Hecht , Dispersion of cryogenic hydrogen through high-aspect ratio nozzles, International Journal of Hydrogen Energy 46 (23) (2021), 12311-12319
21. A. Friedrich, W. Breitung, G. Stern, A. Veser, M. Kuznetsov, G. Fast, B. Oechsler, N. Kotchourko, T. Jordan, J.R. Travis, J. Xiao, M. Schwall, M. Rottenecker, Ignition and heat radiation of cryogenic hydrogen jets, International Journal of Hydrogen Energy 37 (2012), 17589-17598
22. S.H. Han, D. Chang, J.S. Kim, Release characteristics of highly pressurized hydrogen through a small hole. International Journal of Hydrogen Energy 38 (2013), 3503-3512
23. L. Gong, S. Yang, Y. Han, K. Jin, L. Lu, Y. Gao, Y. Zhang, Experimental investigation on the dispersion characteristics and concentration distribution of unignited low-temperature hydrogen release, Process Safety and Environmental Protection, 160 (2022), 676-682